Pergamon

Geochimica et Cosmochimica Acta, Vol. 68, No. 14, pp. 3079–3094, 2004

0016-7037/04 $30.00 + .00

doi:10.1016/j.gca.2004.01.014

Revealing forms of iron in river-borne material from major tropical rivers of the Amazon Basin (Brazil)

T. Allard,[1,*] N. Menguy,[1] J. Salomon,[2] T. Calligaro,[2] T. Weber,[1] G. Calas,[1] and M. F. Benedetti[3]

[1]Laboratoire de Minéralogie-Cristallographie, UMR 7590 Universités Pierre & Marie Curie et Denis Diderot, IPGP case 115, 4 Place Jussieu, 75252 Paris Cedex 05 France

[2]Centre de Recherche et de Restauration des Musées de France, Palais du Louvre, Paris Cedex 01 France

[3]CNRS UMR 7047 Laboratoire de Géochimie et Métallogénie, Université Pierre & Marie Curie, 75252 Paris Cedex 05 France

(*Received October* 15, 2003; *accepted in revised form January* 28, 2004)

Abstract—The present study deals with the direct determination of colloidal forms of iron in river-borne solids from main rivers of the Amazon Basin. The contribution of different forms of colloidal iron have been assessed using ultrafiltration associated with various techniques including electron paramagnetic resonance spectroscopy (EPR), high resolution transmission electron microscopy (HRTEM), and micro proton-induced X ray emission analysis (μPIXE). EPR shows the presence of Fe^{3+} bound to organic matter (Fe^{3+}-OM) and colloidal iron oxides. Quantitative estimate of Fe^{3+}-OM content in colloidal matter ranges from 0.1 to 1.6 weight % of dried solids and decreases as the pH of the river increases in the range 4 to 6.8. The modeling of the field data with the Equilibrium Calculation of Speciation and Transport (ECOSAT) code demonstrates that this trend is indicative of a geochemical control resulting from the solubility equilibrium of Fe oxyhydroxide phase and Fe binding to organic matter. Combining EPR and μPIXE data quantitatively confirms the presence of colloidal iron phase (min. 35 to 65% of iron content), assuming no divalent Fe is present. In the Rio Negro, HRTEM specifies the nature of colloidal iron phase mainly as ferrihydrite particles of *circa* 20 to 50 Å associated with organic matter. The geochemical forms of colloidal iron differentiate the pedoclimatic regions drained by the different rivers, corresponding to different major weathering/erosion processes. Modeling allows the calculation of the speciation of iron as mineral, organic and dissolved phases in the studied rivers.

1. INTRODUCTION

The understanding of forms of iron and their various biogeochemical interactions remains an important issue in environmental science (Davison and De Vitre, 1992; Warren and Haack, 2001). Indeed, available Fe is an essential element for numerous biotas, including phytoplancton (Wells, 1999). In addition, colloidal iron oxides are known to play an important role on the mobility and bioavailability of various metals, through their reactivity, their high surface area, and ubiquity at the Earth's surface (Warren and Haack, 2001). The recognition of iron chemical and mineralogical species in natural systems is critical for a predictive modeling of Fe speciation involving water, mineral, and organic compounds, as related relevant field and experimental data are still sparse (see e.g., Tipping et al., 2002). Recent modeling efforts (Kinniburgh et al., 1999; Tipping et al., 2002; Milne et al., 2003) have provided generic Fe as well as Al binding parameters towards natural organic matter analogues (i.e., humic and fulvic acids). Because these models are calibrated with a limited database with poor statistics that covers a limited pH range, they still have to prove their ability to describe complex geochemical environments in a reasonable way.

The presence of nanometric iron-bearing phases in natural waters in the former operationally defined 'dissolved' fraction (i.e., passing through 0.45 or 0.2 μm filter) is now widely accepted, lowering the limit of 'truly' dissolved fraction down to one nanometer (Buffle and van Leeuwen, 1992). Various colloidal forms of iron have then been observed or postulated in freshwater and marine water, which account for iron concentrations commonly several orders of magnitude larger than the equilibrium solubility of iron oxyhydroxides. In oxygenated freshwaters, forms of iron currently consist in organic complexes of iron and nanometric Fe-rich phases e.g., oxyhydroxides or phosphates (Davison and De Vitre, 1992). Especially, organic-rich rivers are known to exhibit high iron concentrations resulting from strong Fe-organic matter interaction, although actual related Fe forms were not documented (Eyrolle et al., 1996; Viers et al., 1997). Direct evidence of nanosized Fe oxides and Fe(III) bound to colloidal organic matter in tropical organic-rich streams were obtained using electron paramagnetic resonance spectroscopy (EPR) (Olivié-Lauquet et al., 1999; Olivié-Lauquet et al., 2000). The combination of EPR calibration experiment and total Fe content in suspended solids yielded estimates of related distribution of Fe forms in particulate and colloidal fractions, showing the significant contribution of Fe oxides. Besides, Fe(III) bound to organic matter can be revealed indirectly by kinetic methods, providing an estimate of its proportion in freshwater samples, the remaining part of iron being assumed to occur as colloidal oxides (Tipping et al., 2002 and reference therein). A large diversity of iron-rich particles have been described in aquatic systems using transmission electron microscopy, which requires time consuming analyses to get statistically meaningful interpretations (Leppard, 1992). Their association to organic matter appears to be widespread in freshwaters from various origins (Buffle et al., 1998; Perret et al., 2000). The detailed determination of their

* Author to whom correspondence should be addressed (allard@lmcp.jussieu.fr).

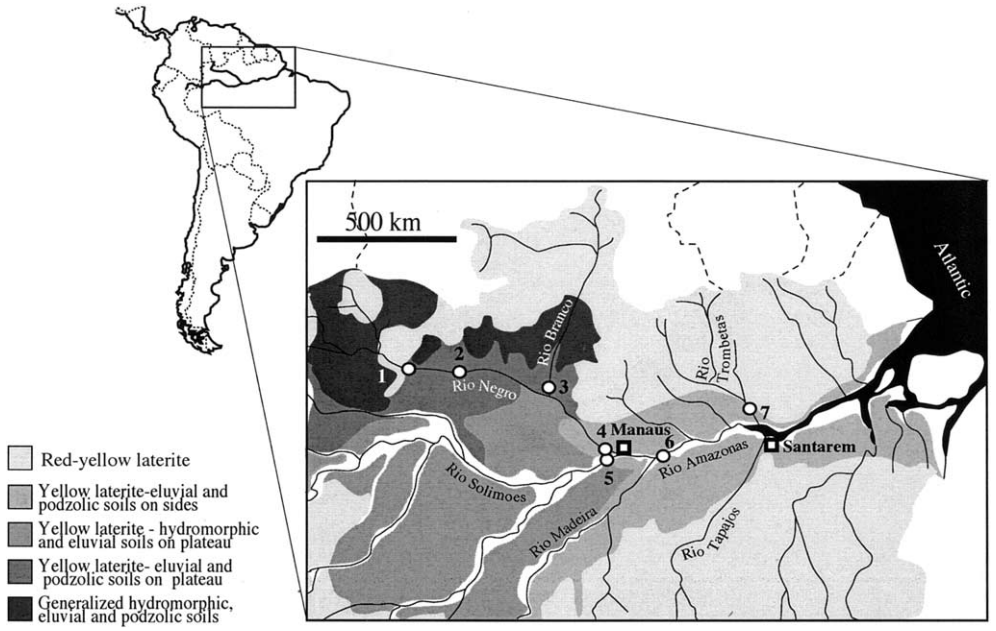

Fig. 1. Location of samples. Lateritic landscapes in the central Amazon Basin, Brazil (simplified according to the pedologic map RADAM Brazil 1/2 500 000).

nature has been scarcely addressed, although this is an important issue for predictive geochemical modeling of their reactivity and stability. This arises mainly from the complexity of characterizing such nanometric particles present at trace concentration in aquatic systems and requiring specific sampling techniques (Perret et al., 1990; Perret et al., 1991). When combined to composition analysis, mineral identification at nanoscopic scale can be achieved using electron diffraction and/or high resolution transmission electron microscopy (HR-TEM) of previously characterized samples, by revealing interplanar spacings characteristic of crystallographic structures (e.g., Fortin et al., 1993; Mavrocordatos and Fortin, 2002). This has proved to be relevant for structural identification of short ordered iron oxides such as ferrihydrites (Banfield et al., 2000; Janney et al., 2000a; Janney et al., 2001).

The present study focuses on naturally occurring forms of iron in suspended material from major rivers of the central Amazon Basin. This basin represents a giant collector of weathering products and erosion material originating from several distinct pedoclimatic regions. The central basin is largely covered by laterites with various stages of degradation related to hydromorphic, eluvial, and podzolic processes (Fig. 1; Dubroeucq and Volkoff, 1998; Fritsch et al., 2002). Related rivers exhibit a wide variety of physical and chemical parameters originating from the different erosion regimes and sources of materials (Sioli, 1984). The Amazon River drains more than 6.10^6 km^2 and has an average discharge of 209000 m^{3}s^{-1}, supplying up to 20% of all the river discharge to the oceans (Molinier et al., 1997). Therefore, the Amazon River system is a prominent link in global carbon and metal ion cycles, and understanding its aqueous geochemistry is of considerable importance. Average Fe concentrations are ~89 μmolL^{-1} in river water and 0.53 μmolL^{-1} in water filtered with 0.45 μm pore size (Gibbs, 1972; Gibbs, 1977; Benedetti et al., 2003a). Consequently, the corresponding iron export rates of the Amazon to the ocean are huge, nearly 587 10^9 moles yr^{-1} and 3.5 10^9 moles yr^{-1} for raw and filtered water samples, respectively. A dominant part of iron (>95%) is transported in the particulate fraction (>0.2 μm) for various rivers of the basin including Rio Negro and the Amazon River, the remaining Fe being mainly in the colloidal fraction (0.2 μm-5 kilo Daltons (kD)) (Allard et al., 2002, Benedetti et al., 2003a). A few studies were devoted to the nature of transported solids and related forms of iron, but so far, no relation was made with river chemistry or erosion processes. According to estimates by Gibbs (1973) performed from chemical extraction methods, most iron (>90%) in the Amazon River occurs almost equally as oxides and incorporated in crystalline detrital grains, with a minor contribution of organic forms (6.5%). River-borne solids from various rivers of the Amazon basin have been characterized using ultrafiltration technique and several mineralogical, spectroscopic, and chemical methods (Allard et al., 2002; Benedetti et al., 2003b). The particulate (>0.2 μm) fraction was organo-mineral, with mineralogy consistent with previous studies (Irion, 1991; Martinelli et al., 1993). By contrast, the colloidal fractions (0.2μm-5 kD) were dominantly composed of "humic"-like material with various contents of iron. According to Benedetti et al. (2003a), iron is dominantly (>95%) distributed in the particulate fraction and below 0.2 μm, the colloidal fraction accounts for more than 70%. Besides, fractions and forms of organic carbon have been characterized in numerous studies (e.g., Hedges et al., 1992; 1994; Benedetti et al., 2002). Carbon is significant as colloidal matter in the Rio Negro (30 to 40% of TOC) whereas it is dominantly present in the dissolved (<5 kD) fraction in the Amazon River (Benedetti et al., 2002; Mounier et al., 2002). The composition of organic matter was studied on various samples from the Rio Negro, Rio Solimoes, and Amazon by Gadel et al. (2000). These authors showed that the average

Table 1. Characterization of samples from the Amazon Basin.

Sample	Location	Water discharge (m^3s)	T (°C)	[SM] (mg/l)	pH	Conductivity (μS/cm)	[TOC] (ppm)	Distribution of organic carbon (%)			[Fe] 10^{-6} (mol/L)	Mineralogy (>0.2 μm fraction)
								P	C	D		
Rio Negro J 07	1-Curicuriaci	12300	27.4	1.2	4.0	21	7.9	7	NM	NM	3.4	
Rio Negro RN-X	2-Foz do Açai	NM	29.0	NM	4.1	19	10.2	11	43	46	3.75	
Rio Branco J 15	3-Foz do Rio Negro	3500	30.6	21.2	6.4	21	3.1	6	32	62	9.3	Kaolinite, quartz, gibbsite
Rio Negro J 20	4-Paricatuba	30500	30.6	2.5	4.5	10	8.7	13	40	47	6.8	
Rio Solimoes	5-Manaus	NM	30.3	NM	5.9	94	3.9	NM	NM	NM	29.3	Smectite, illite, kaolinite, chlorite, quartz, feldspars
Rio Amazonas J24	6-Itacoatiara	88695	29.8	28.2	6.8	70	3.9	5	35	60	10.0	
Rio Trombetas J25	7-Oriximina	500	34.5	4.9	6.1	18	NM	NM	NM	NM	3.4	Kaolinite, quartz, gibbsite, smectite

[SM] = suspended matter (>0.2 μm) content; [TOC] = total organic carbon content; P = particulate fraction; C = colloidal fraction; D = dissolved fraction; NM = not measured.

proportion of carbon from polysaccharides is minor, i.e., ~4% for particulate and colloidal fractions.

In the present study, one main objective is to directly evidence different forms of iron in the organo-mineral material transported by different rivers of the Amazon Basin, with particular attention to the colloidal fractions, including their relation to the chemical parameters of the rivers. With this aim in view, a combination of physical and chemical methods are used, including spectroscopic analyses of solids by EPR, compositional analyses of small samples by Particle Induced X-ray Emission (PIXE), and analysis of nanosized iron oxides by HRTEM. The obtained results are compared to the prediction of geochemical codes assuming iron organic matter/mineral/solution equilibrium. Results are discussed in terms of geochemical significance of Fe solid species and stability of colloidal oxides.

2. GEOCHEMICAL BACKGROUND

A variety of physical and chemical characters have long been recognized for the rivers of the Amazon basin, and different classifications have been proposed to account for the white, clear, and black waters encountered in the field (Sioli, 1984; Lewis et al., 1995). Schematically, clear and black waters are mainly related to chemical erosion, whereas white waters contain much stronger sediment loads inherited from mechanical erosion. The white waters from the Amazon River and its upper stream Rio Solimões carry suspended material from the Andes and the corresponding alluvial zone. They drain regions covered by various soils including acrisols, ferralsols, nitisols, and cambisols. Tributaries from the northern side of the central Amazon Basin (e.g., Rio Negro, Rio Branco, Rio Trombetas) correspond to regions of weathering profiles developed on precambrian shield and sediments of different periods, including paleozoic, mesozoic (Alter do Chao), and cenozoic (Solimões) formations. The Rio Negro drains a region of podzol, ferralsol and acrisol supporting a rainforest. Similar environment occurs downstream of the Rio Branco (white waters), but this river also drains a savannah region supported by quaternary sediments in its upper course. The Rio Trombetas (clear waters) is dominantly related to ferralsol and acrisol mainly developed on Precambrian shield. The minerals from the particulate fraction, inherited from soils and rocks of the drained areas, differentiate mainly white waters of Andean origin from rivers of the northern side of the Basin (Table 1).

3. SAMPLES

The studied rivers exhibit contrasting physical and chemical properties such as pH, conductivity, sediments load, and discharge (Table1). Samples analyzed by spectroscopy were collected during a cruise of the Hidrologia da Bacia Amazonica (Hibam) project in September 1998, corresponding to a falling stage period (Table 1). Surface water samples (−1m) of 50L were collected in the upper part of the Rio Negro and before its mixing with the Amazon river, in the Rio Branco, the Rio Solimões, the Rio Trombetas and the Amazon (Fig. 1). Water samples were processed onboard using tangential-flow ultrafiltration (Ultrasart, Sartorius Inc.), with membranes of nominal cutoffs at 0.2 μm and 5 kD. All membranes had been cleaned in the laboratory with 50 L of Milli-Q water. In the field the first 5 L were processed and discarded to prevent sample contamination during filtration. Concentration factors ranged from 8 to 15. Detailed information on the tangential-flow ultrafiltration procedure and mass balance calculations can be found elsewhere (Eyrolle et al., 1996; Benedetti et al., 2003a). Hereafter, the fractions above 0.2 μm, between 0.2 μm and 5kD, and below 5 kD stand for the particulate (P), colloidal (C) and dissolved (D) fraction, respectively. Aliquots of the unfiltered water, permeates, and filtrates were stored at 4°C after addition of NaN_3 (1 $mmolL^{-1}$) to prevent bacterial development before total organic carbon analysis. Similar aliquots were acidified (pH 1) with ultrapure HNO_3, for major and trace elements determination by Inductively Coupled Plasma-Atomic Emission Spectroscopy (ICP-AES). Recovery process of dried solids from the filtered fractions is an important step for subsequent reliable analysis by EPR spectroscopy and PIXE, as it may induce artifacts such as precipitates from solution, particularly in colloidal samples for which the concentration is low (Hart et al., 1993; Olivié-Lauquet et al., 2000). Suspended solids were

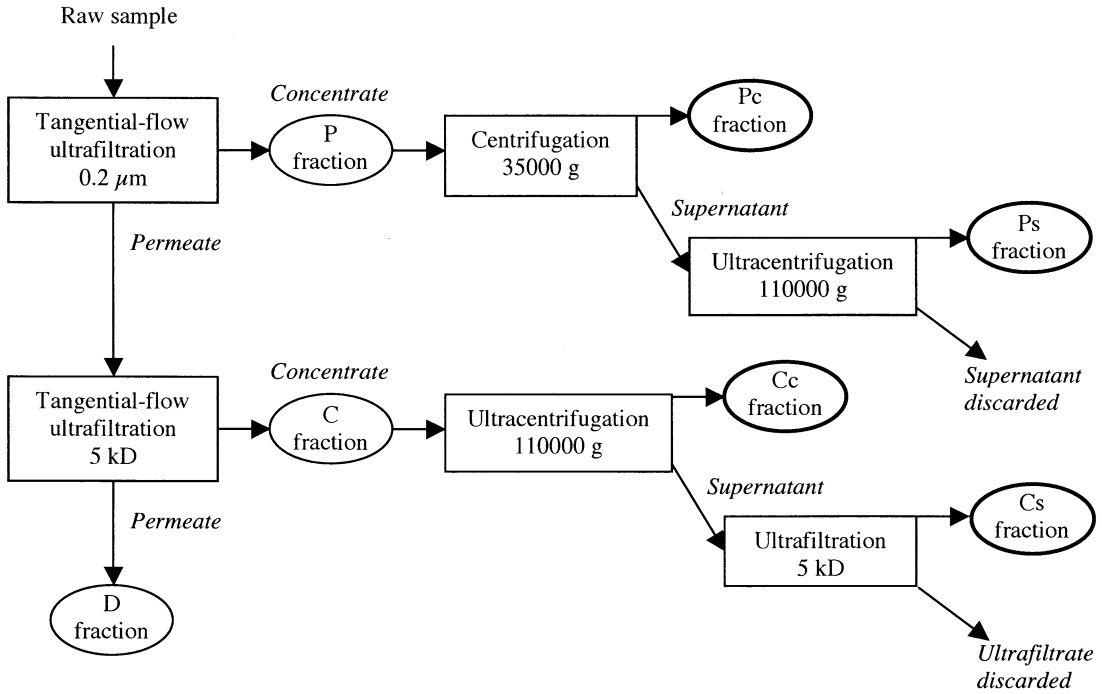

Fig. 2. Scheme of sample preparation. Plain and bold circles indicate water and solid samples, respectively.

recovered without any chemical pretreatment. Before drying, the solids were separated from solution by centrifugation and ultrafiltration (Fig. 2), to minimize the contribution of chloride salts, silica, and organic carbon from the solution (i.e., dissolved form) during the drying step. Indeed, these contributions may account for, e.g., 10 to 50 mg/L in the Rio Negro and Solimões.

Solids were separated at the laboratory by centrifugation, operating at 35 000 g (1 h at 20°C) and 110 000 g (17 h at 10°C) from P and C fractions, respectively. Related recovered solids are refered to as Pc and Cc fractions, respectively (Fig. 2). Nevertheless, some organic-rich material remained suspended in the supernatants owing to its low density. These supernatants obtained from P and C fractions were then separated by centrifugation at 110 000 g and by ultrafiltration at 5 kD with ultrafree Sartorius units, respectively. Related recovered solids are refered to as Ps and Cs fractions, respectively (Fig. 2). All concentrates were then oven dried overnight at 35°C. The main bias arising from the preparation of samples, i.e., filtration, centrifugation, and drying is expected to be an increasing degree of aggregation of particles. The colloidal sample from the river Amazon (Ct) was recovered by drying the concentrate without separating subfractions of the colloidal material, owing to the low amount of collected material. Although losses of materials occurred on ultrafiltration membranes, mass proportions of recovered solids can be given indicatively. Thus, the proportion of colloidal fraction, among which the Cc fraction was minor, was less than 10%, except for the Rio Negro where it accounted for 10 to 60%. Materials from supernatants of particulate fractions (Ps samples) were significant only for the Rio Negro, owing to the presence of organic matter. However, recovery balance was not fulfilled satisfactorily enough because of losses occurring on filtration membranes as a result of clogging or sorption (see e.g., Buffle and van Leeuwen, 1992), particularly concerning iron. This hindered the possibility of measuring iron distribution in the various fractions.

4. MATERIAL AND METHODS

EPR measurements were performed at 9.42 GHz (X-band) frequency with a Brucker ESP300E. The spectra were recorded at 145 K with a cooled nitrogen flow device, to enhance paramagnetic transitions to the detriment of superparamagnetic signals. Measurements were conducted using a microwave power of 40 mW, modulation amplitude of 3 to 5 gauss and normalized filling factor of the resonant cavity. Data were normalized according to gain and sample mass. Effective values of spectroscopic factor g are calibrated with DPPH (g = 2.0037). The resonance relation for EPR is given by:

$$h\nu = g\beta H$$

or

$$g = 0.714484\nu/H$$

Where h is the Planck constant, ν is the hyperfrequency (MHz), β is the Bohr magneton and H the magnetic field (gauss).

TEM experiments were performed on a Jeol 2010F microscope operating at 200 kV and equipped with a high resolution UHR pole piece. Low magnification investigations have been carried out using a high defocus value and elastically scattered electrons, providing pictures of weak phase object such as organic matter. EDS analyses were performed using a Kevex detector with an ultrathin window. TEM samples were prepared onboard without staining, according to the procedure described in Perret et al. (1991). This procedure allows fixing the organo-mineral associations of river-borne particles, and was also shown to preserve organization and structure of poorly ordered nanometric Fe oxides (Greffié et al., 2001). A drop of river water was mixed with hydrophilic resin then spread over a Cu grid by horizontal centrifugation, before polymerization in a desiccator. The TEM analyses were performed on samples from Rio Negro.

PIXE analyses were performed on a Van de Graaff accelerator at the

Table 2. Selected PIXE analyses of particulate (Pc, Ps) and colloidal (Cc, Cs) fractions, expressed in ppm unless specified.

		Rio Negro (J20)				Rio Branco (J15)				Rio Negro (RNX)			Rio Amazonas	
	LOD	Pc	Ps	Cc	Cs	Pc	Cc	Cs	Pc	Ps	Cc	Cs	Pc	Ct
Si	26	55300	896	9287	215	87733	43307	1260	51567	380	4919	308	75600	3682
Al	45	43676	3362	3971	3415	49394	10535	762	41824	2695	4341	3034	39727	259
Fe	28	24430	24430	8540	13125	26950	8260	3395	16800	11900	7490	10115	26180	700
Na	119	2767	6195	21145	4340	875	23148	7123	6240	18548	20848	7197	2374	47632
Mg	72	1218	2328	2388	2976	1422	4170	4974	1209	804	1782	2124	3468	5382
K	25	4066	1411	6414	1784	7841	10372	2921	5045	1369	4796	1900	10787	5560
Ca	36	1964	9071	7643	13286	1607	11643	22786	1286	5250	5093	8286	3421	41714
Ti	12	2490	120	294	126	2460	870	96	3522	63	141	60	2010	39
Mn	15	147	434	504	767	519	147	15	93	190	287	480	395	0
P	39	332	114	201	0	192	157	0	192	43	127	0	188	0
S	20	608	1020	1160	800	148	1800	1556	580	756	896	640	180	10536
Cl	40	695	480	1500	490	105	1750	640	375	585	865	620	205	8250
Cu	3	14	22	31	53	22	46	124	17	38	39	45	26	70
Total Oxide %		49	11	15	9	66	36	10	46	9	12	8	59	28
Total Organic %		51	89	85	91	34	64	90	54	91	88	92	41	72
[OM]* %		33	85	87	85	40	NM	NM	32	94	NM	91	44	NM

[OM]* = organic matter content analyzed by carbon element analyzer; LOD = limit of detection; NM = not measured.

Musée du Louvre (Paris), using an external beam of 3 MeV protons. Small pellets of 1mm diameter and ~0.5 mg were prepared with dried material and positioned in the beam under He flux (5 L/min flow rate). The beam was scanned over ~200 × 200 μm^2. X-rays were measured with two SiLi detectors for major and trace elements, respectively. A diorite standard (DRN) from NIST was used for quantitative element analysis. PIXE data were fitted using the GUPIX code (Maxwell et al., 1989). The contribution of organic matter was taken into account by assuming a simplified composition of humic acid ($C_{38}H_{39}O_{23}$) from Suwanee river (Mills et al., 1996).

The total organic carbon (TOC) was determined in water samples using a Shimadzu TOC analyzer that utilized a high temperature oxidation procedure with IR detection. The detection limit was 0.1mgL^{-1} and the precision ranged from 5 to 10%. Chemical analyses of total iron in water were performed with Inductively Coupled Plasma-Atomic Emission Spectroscopy measurements (ICP-AES) on a 238 Jobin Yvon spectrometer (see Benedetti et al. (2003a) for details on analytical measurements).

When enough solid was available, carbon analyses of recovered solid fractions were performed on a Carlo-Erba NA-1500 NC Elemental Analyser at the Laboratoire de Biogéochimie Isotopique (Paris, France). The organic matter content was estimated by a conversion factor of 2, corresponding to the average mass-ratio of C in humic substances (Swift, 1996). A a matter of fact, according to Gadel et al. (2000), the polysaccharide content in our samples was assumed to be minor.

5. RESULTS

5.1. Composition of Suspended Solids

The average concentrations of suspended matter in the rivers differentiate the white rivers for which [SM] is relatively high, from the black and clear rivers for which [SM] is relatively low (Table 1). This is in agreement with inheritance of relatively strong mechanical erosion in the white waters. In addition, the proportions of organic carbon in P, C, and D fractions of water samples are given in Table 1. It is mainly shown that the C fraction is significant for the Rio Negro samples whereas the D fraction is dominant for the other white rivers such as Rio Branco and Rio Amazonas.

The chemical compositions of particles were determined on some samples by μPIXE analyses (Table 2). They are described by reference to the previous determination of the nature of suspended materials by Allard et al. (2002). Selected data are plotted in a ternary diagram Si+Al/Fe/Na+Mg+K+Ca and expressed in Mol %, to differentiate size fractions and origin of particles (Fig. 3).

The major components of the particulate Pc fractions include Si, Al, and to a lesser extent Fe, as expected from the mineralogical composition of these fractions which typically include clays, residual minerals (e.g., quartz), and iron oxides. Accordingly, the Pc samples plot close to the Si+Al end member and separately from the other fractions (Fig. 3).

By contrast, in the Ps and colloidal fractions, Na, Ca, and to a lesser extent Fe, become dominant (Table 2). The organic fractions from the Rio Negro (Ps and Cs) distinguished themselves from the other samples by their higher Fe content (Fig. 3). In addition, Si is significantly present in the Cc fraction only, particularly in the sample from the Rio Branco. This is in agreement with the previous observation of colloidal kaolinite by FTIR in this fraction (Allard et al., 2002). Nevertheless, the excess of Si over Al indicates that minor Si-rich components (e.g., amorphous silica) exist, though not differentiated through FTIR.

The organic matter content mostly differentiates the Pc fractions, for which the mineral content is significant, from the other fractions that are organic-rich. For the Pc fractions from the Rio Negro, the contribution of organic matter reconstructed by PIXE is overestimated, as can be seen when compared to that estimated from carbon analyses (Table 2). This discrepancy may be due partly to an inaccurate model for the organic matter composition, i.e., overestimating the amount of carbon. As a matter of fact, the conversion factor of carbon content is obviously dependent of the organic matter composition. A value as high as 2.5 can be assumed in soils and it would yield more consistent results (Nelson and Sommers, 1996). Further chemical characterization of organic matter is necessary to test this hypothesis. By contrast, the Ps and colloidal fractions show the prevalence of organic matter that quantitatively supports the previous observation of “humic” like organic matter by FTIR. These fractions show a better agreement between the two sets

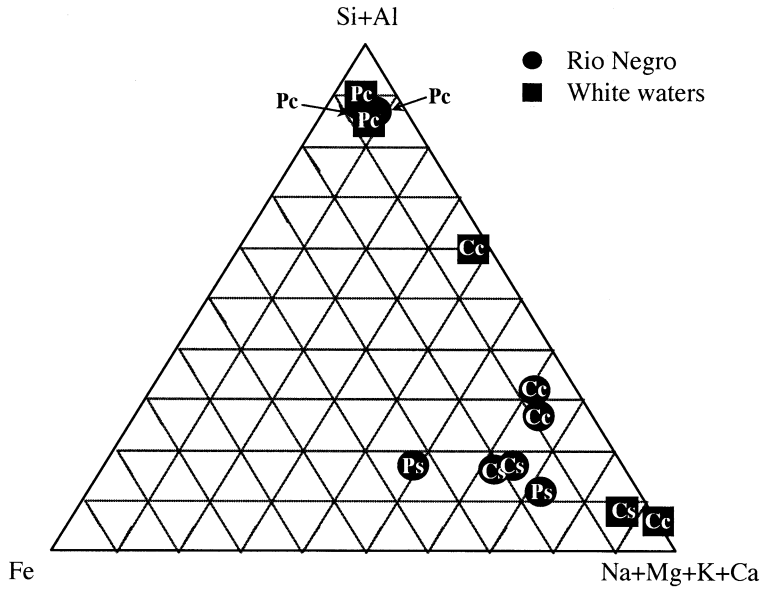

Fig. 3. Composition of samples analyzed by μPIXE, expressed in Mol %: Rio Negro (J20 and RNX samples) and white waters from Rio Branco and Rio Amazonas.

of carbon analyses. In these fractions, the Na, Ca, together with part of Al are expected to react with organic matter, owing to the affinity of these elements towards organic functional groups.

Fe is present around and above the percent level, typically within 0.75 to 2.45 weight % of Fe in the Rio Negro. By contrast, the Fe concentration in solids from white rivers (Rio Branco, Amazon River) ranges within 0.07 to 2.7 weight %. Iron is preferentially concentrated in the Pc fraction, where it may occur mainly as oxide and oxyhydroxide phases inherited from eroded soils and sediments. As previously indicated, iron is mainly contained in the particulate fraction of aqueous samples, the proportion of iron in colloidal material being generally minor.

5.2. EPR of Suspended Solids: Forms of Trivalent Iron

5.2.1. Identified species

The EPR spectra of Pc fractions are presented in Figure 4. The signal located at low magnetic field around g = 4.3 (1600 G) arises from magnetically diluted Fe^{3+} present in diamagnetic materials, i.e., mostly the clays (e.g., Goodman and Hall, 1994). In the Rio Solimões and the Amazon river, EPR spectra were similar, reflecting the minor contribution from the Rio Negro, owing to its comparatively lower discharge and sediments load than the Rio Solimões (Table 1).

For the Northern Basin river samples, i.e., from Rio Negro, Rio Branco, and Rio Trombetas, the g ≈ 4 region exhibits signals characteristic of structural iron in kaolinite (Balan et al., 1999). A superimposed contribution due to Fe^{3+} bound to organic matter was also observed, particularly in the Rio Negro samples. This contribution was previously revealed after organic matter removal by oxidative treatment (Allard et al., 2002). The corresponding spectrum is clearly seen without mineral interference in Ps, i.e., organic-rich, fraction. It is characterized by a rhombically distorted signal with intense resonance at g = 4.3, typical of magnetically diluted high-spin Fe^{3+} ions bound to carboxylic or phenolic type groups of the

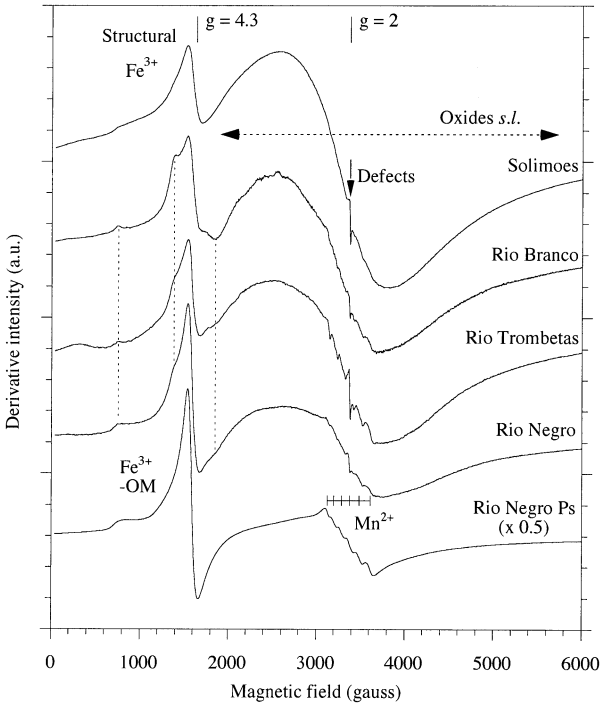

Fig. 4. EPR spectra of particulate fractions. Various species are observed: structural Fe^{3+}, Fe^{3+} complexed to organic matter (Fe^{3+}-OM), iron oxides *sensu lato*, i.e., including oxyhydroxides, and associated divalent manganese. Dotted lines show the main transitions of structural Fe^{3+} in kaolinite. Spectra were recorded at 145 K.

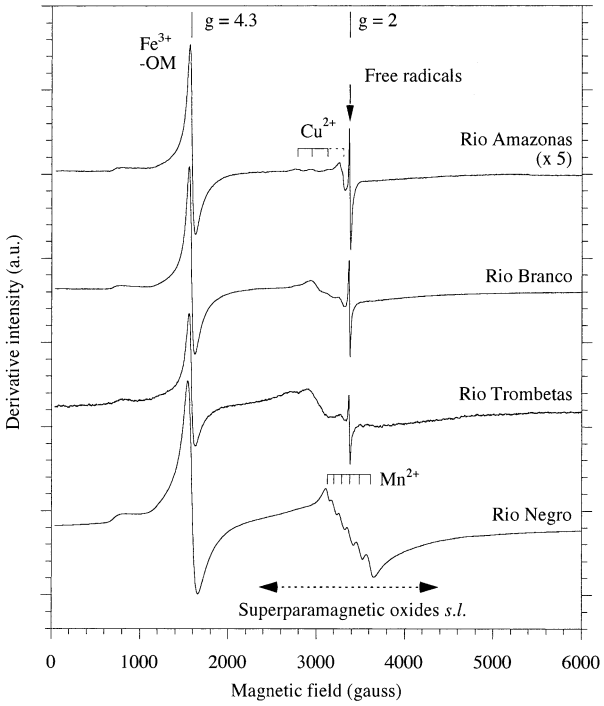

Fig. 5. EPR of colloidal material (Ct fraction for the Amazon and Cs fractions for the other rivers). See text and Figure 4 for legend of identified species. Spectra were recorded at 145 K.

organic matter as inner sphere complexes (Senesi, 1992). From here and after, this iron species is referred to as Fe^{3+}-OM.

All samples of Pc fractions also show a strong and broad (>1000 gauss) resonance centered at g = 2 (3500 G) with varying amplitude. This is related to iron oxides and oxyhydroxides, either isolated or associated with clays as embedded particles or coatings (Muller and Calas, 1993).

At g = 2 (around 3400 G), a narrow and weak signal is related to radiation-induced defects, accumulated in kaolinite from any environment (Clozel et al., 1994). Besides, the Ps sample from the Rio Negro clearly exhibits a six-line signal centered at g = 2, that is due to the hyperfine structure of Mn^{2+} ions associated with organic matter as outer sphere complex (Allard et al., 2002). Both the relatively higher concentration of Mn^{2+} in the Rio Negro samples with respect to other studied rivers (Table 2), and the affinity of this ion for organic matter, support this observation.

Figure 5 presents representative spectra of colloidal samples recorded at low temperature (145 K) to enhance the contribution of paramagnetic species. When compared to room temperature spectra (Allard et al., 2002), the present data confirm that river colloids contain specific paramagnetic species such as stable organic-free radicals, Mn^{2+} in the Rio Negro samples and, in the Amazon sample, colloid-bound Cu^{2+}. Nevertheless, all colloid samples are characterized by the presence of Fe^{3+}-OM complexes, the signals of which vary through their width and amplitude. These variations are related to the concentration of iron bound to organic matter in the colloidal material. Moreover, a broad resonance centered near g = 2 with moderate amplitude appears as a common feature to the colloidal samples. It is due to magnetically concentrated domains arising from Fe clusters and oxides in the broad sense, i.e., irrespective of their actual structure or composition. When compared to the room temperature data (Allard et al., 2002), the present spectra show an intensity decrease at 145 K, which is typical of a superparamagnetic behavior and indicative of the nanometric size range of these phases (Bonnin et al., 1982). This behavior is also observed for the particulate organic fraction (Ps) of Rio Negro.

5.2.2. *Trivalent iron bound to organic matter*

The EPR data were used to estimate the concentration of Fe^{3+} bound to organic matter ([Fe^{3+}-OM]) using a calibration performed from experimental sorption of trivalent iron onto a standard humic acid (Olivié-Lauquet et al., 1999). The linear relationship observed up to ~1.2 wt % Fe, despite the presence of Fe nano-oxides associated with organic matter, indicates a slight overestimation of [Fe^{3+}-OM]. In the studied samples from the Amazon basin, the concentration of Fe^{3+}-OM was determined from the main EPR resonance at g = 4.3 using the simplified relation:

$[Fe] = k * \Delta H^2 * I$, which provides an estimate of the area of integrated peak, where k is a constant, ΔH and I are the peak-to-peak line width and amplitude, respectively (Calas, 1988). It is expressed herein in Fe weight percent of dried solid (Fe^{3+}-OM wt %d.s.) for the organic-rich samples, i.e., Ps, Cc and Cs fractions.

The values for the set of samples range from 0.1 to 1.6 Fe^{3+}-OM wt %d.s. and are plotted in Figure 6 as function of pH. For comparison, relevant data on colloidal samples from organic-rich streams in Cameroon (Mengong and Nyong) are also reported, after Olivié-Lauquet et al. (1999). Corresponding EPR spectra were similar to those from the Rio Negro. These values show a decreasing trend with increasing pH, with end members represented by samples from the Rio Negro and the Amazon River, irrespective of the total Fe concentration in the sample (Table1). In the Cc fractions recovered for samples from the Rio Negro and the Rio Branco, [Fe^{3+}-OM] plot 2 or 3 times below their Cs counterparts. Corresponding concentrations range from 0.3 to 0.5 Fe^{3+}-OM wt %d.s., thus showing a weak variation with pH. This trend is underlined separately from the other samples in Figure 6. Two interpretations are considered for the observed discrepancy between Cc and Cs samples. First, a dilution effect of organic matter by mineral components in Cc fraction is possible for the Rio Branco sample, according to the PIXE analyses reported in Table 2. By contrast, this interpretation does not hold for the two Rio Negro samples, for which the organic matter content of Cc and Cs fractions are close. Thus, the present result on Rio Negro colloids rather indicates that the fraction Cc has a lower Fe binding capacity than the Cs and Ps fractions, although no difference was observed by previous FTIR analysis (Allard et al., 2002).

As Cc fraction was minor, and considering the above properties, the pronounced trend observed for other samples as a function of pH (Fig. 6) is representative of recovered substances in the water samples. It reveals a geochemical control on the association of Fe^{3+} with suspended solids. It also differentiates the colloids as a function of the river chemistry. Data points are distributed between those corresponding to

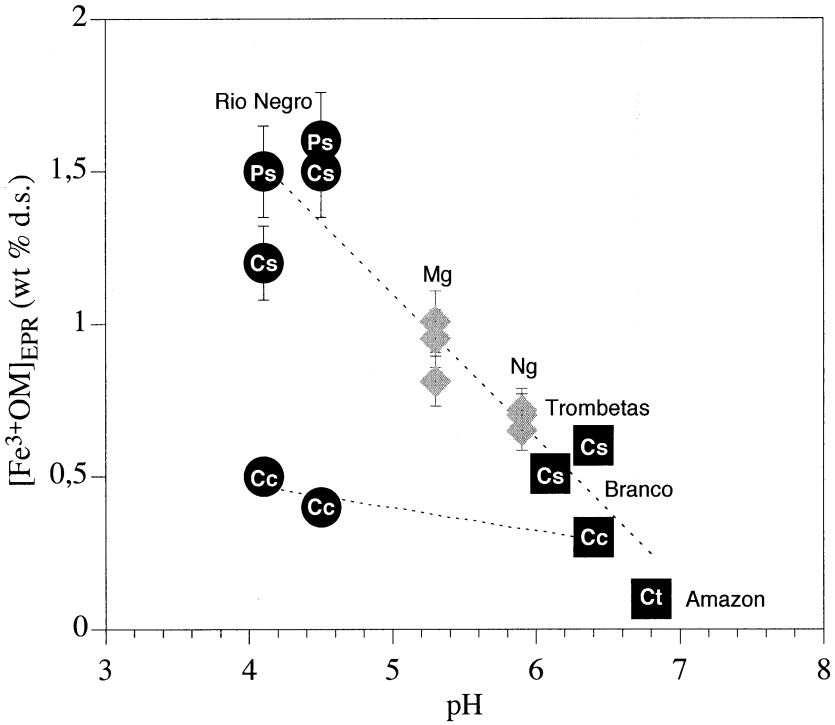

Fig. 6. Concentration of Fe^{3+} complexed to organic matter ([Fe^{3+}-OM]) estimated by EPR as a function of river pH and expressed in weight % of dried solid. Additional data after Olivié-Lauquet et al. (1999), for colloidal samples from organic streams in Cameroon (Mg: Mengong; Ng: Nyong).

black waters with low pH and solute concentrations and those corresponding to white waters with higher pH and solute concentration, those from African rivers being in an intermediate position.

5.3. Quantitative Evidence of Nano Fe-oxyhydroxides

The concentration of Fe^{3+} bound to organic matter (EPR data) is plotted in Figure 7 as a function of total Fe concentration determined by PIXE. Several samples, including all Cs fractions, have values located above the 1/1 line. Thus these data provide an estimate of the total error on EPR determinations, in agreement with the expected overestimation of [Fe^{3+}-OM], and due to calibration in addition to the systematic error on EPR intensity and sample weighing represented by error bars. According to this plot, this overestimation error ranges from10 to 20% for the Fe-rich samples (Rio Negro) and can reach 60% for the less concentrated one (Rio Branco, Cs fraction).

Even without taking EPR error into account, Figure 7 shows that several samples are located well below the 1/1 line. This suggests that iron forms other than magnetically diluted organic complexes are significantly present in the samples. Considering that divalent iron can be neglected owing to the oxidizing conditions prevailing in rivers and during sample collection, this plot reveals the contribution of colloidal iron oxides in the broad sense. The minimum contribution of these phases is within 35 to 65% of total Fe concentration for the samples from the Amazon Basin, and 23% for the Cameroon sample. This supports the observation of superparamagnetic resonances on EPR spectra of colloids and the presence of such nanophases associated with the particulate organic matter (Ps fraction) from the Rio Negro. All data of Cc fractions plot below the 1/1 line, suggesting that iron oxides are concentrated by the ultracentrifugation process.

5.4. TEM Analysis of Nano Fe-oxyhydroxides

Representative transmission electron micrographs are presented for the Rio Negro (Fig. 8). Special attention is brought to organic and iron oxides particles, other mineral components of suspended materials being determined in previous studies (Allard et al., 2002).

In the Rio Negro, different forms of organic material with typical low electron densities are differentiated from their aggregate morphologies. Some organic particles occur as fibrils of a few nm widthforming networks over hundreds of nanometers that are typical of biopolymers derived from microorganisms (Fig. 8 a). In addition, unstructured gel-like domains of organic matter with diffuse contours are also observed, either in association with biopolymers or as isolated entities (Fig. 8a, arrows). These compounds correspond to classes of NOM particles currently recognized in various aquatic systems (Buffle et al., 1998).

Colloidal iron-bearing phases are detected through their higher electron density and composition by EDS analysis. They correspond to nanometric particles (typically a few nm) either isolated or aggregated over short distance, and most often associated with biopolymer and diffuse organic matter domains. These characteristics precluded traditional analysis by

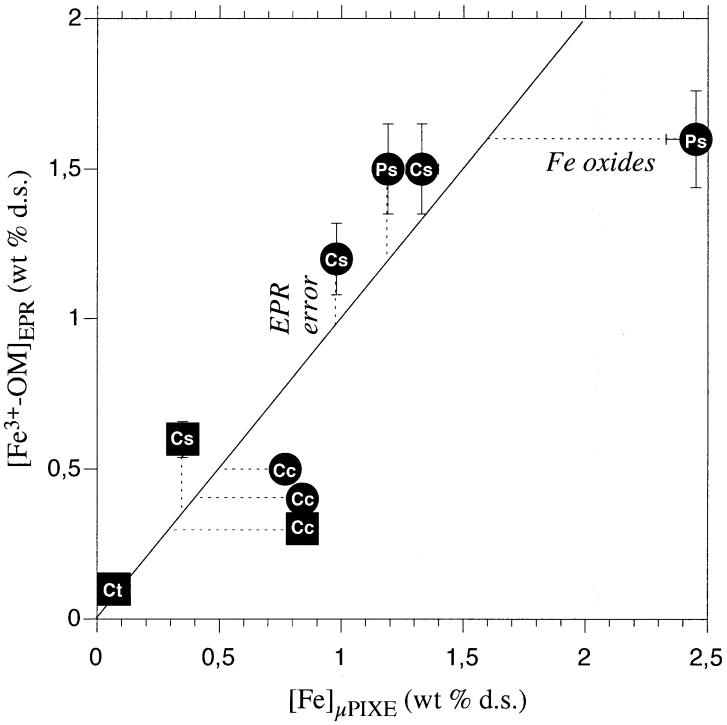

Fig. 7. Relation between concentration of Fe^{3+} complexed to organic matter estimated from EPR and total Fe content determined by μPIXE (concentrations expressed in weight % of dried solid). Circles and square represent samples from the Rio Negro and white rivers, respectively. Position of data with respect to the 1/1 line is related to the EPR error (including systematic and calibration error) and the contribution of colloidal iron oxides *sensu lato.*

conventional electron diffraction. By contrast, HRTEM analyses of these particles revealed their nanocrystalline nature and provided structural constraints on phase identification. The direct observation of these nanometric iron-rich colloids is in agreement with the identification of superparamagnetic phases by EPR. Typical examples of particles are described below.

In Figure 8a, a branched aggregate is shown in association to a fibril network, suggesting that nucleation of iron oxides was favored by organic structures. The corresponding Fourier transform of the HRTEM image evidences a poorly ordered phase (Fig. 8b), with interplanar spacings at 0.245 nm. These parameters are consistent with two-line ferrihydrite, a poorly ordered iron hydrous ferric oxide commonly encountered in surface environments (Jambor and Dutrizac, 1998; Janney et al., 2000b). However the other characteristic distance at 0.15 nm was not observed. A sample from the Cc fraction redeposited on a grid was also observed, to search for the iron bearing phases suggested by EPR and PIXE analytical results presented in Figure 7. As shown in Figure 8c, this sample contained 20 to 30 Å nanocristalline oxyhydroxides assembled in a compact aggregate, with no preferential orientation. Here, aggregation mode is not thought to be a relevant parameter since it may result from the centrifugation process. The FT of the HRTEM image also reveals lattice fringe spacings around 2.5 Å and 1.5 Å, consistent with ferrihydrite.

In addition to iron and oxygen, EDS analysis occasionally reveals the presence of various amounts of associated silicon. Silica is known to be a common impurity in natural ferrihydrites (Jambor and Dutrizac, 1998), as well as in unidentified colloidal iron oxides from freshwaters (Perret et al., 2000).

A rare occurrence of oriented arrangement of nanoparticles was observed, as shown in Figure 8d. This particular arrangement suggests epitactic growth, a mode of formation that was recently identified in natural oxyhydroxides (Banfield et al., 2000). HRTEM lattice fringe spacings are revealed at 2.6 to 2.45 Å on the FT image. Such distances are consistent with various oxides and oxyhydroxides including ferrihydrite. The EDS spectrum of these particles showed the presence of sulfur in low amount with respect to Fe. Despite the relatively high S/Fe ratio (0.1–0.25) revealed by PIXE analyses, the possibility of occurrence of schwertmannite, an oxyhydroxysulfate currently observed in acid sulphate-rich waters was not preferred because its X-ray diffraction peaks are different (Bigham et al., 1994; Bigham et al., 1996). Consequently, sulfur most likely occurs as oxyanions adsorbed onto ferrihydrite and as a component of organic matter. Indeed, sulfate anions exhibit strong affinity for ferrihydrite surface, the related mechanism being demonstrated by EXAFS, showing that the oxyanion coordinates directly through inner sphere complexation onto surface sites (Manceau and Charlet, 1994).

Besides nanometric iron oxyhydroxide phases, Fe is found associated at trace level to colloidal kaolinites in the Rio Negro. Kaolinites with size around 100 nm are observed (Fig. 8 e), in agreement with their previous identification by FTIR in the Cc fraction. Their euhedral shape indicates that they are not affected by weathering. Both the low content of Fe in kaolinite

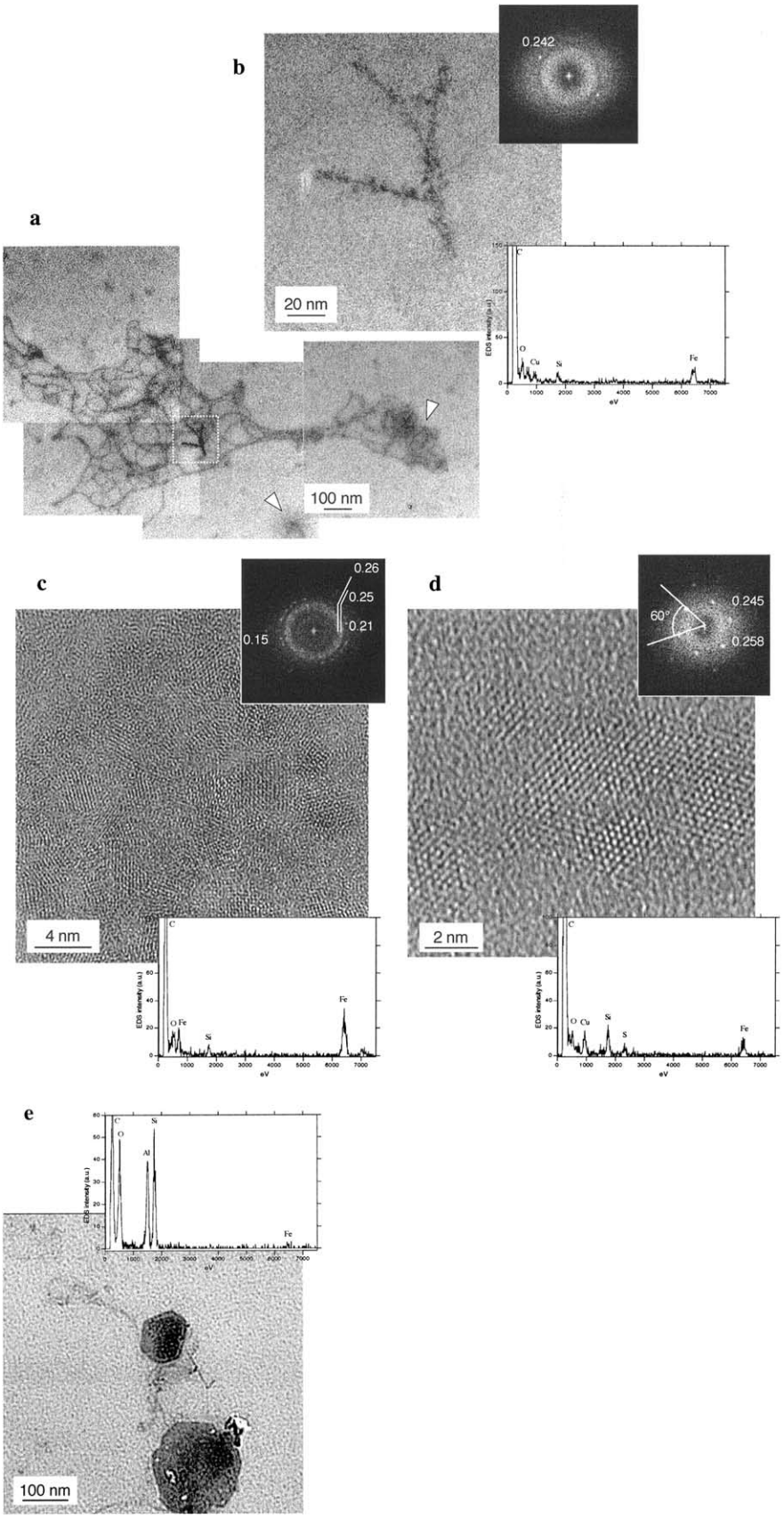

Fig. 8. TEM observation of river-borne particles from the Rio Negro. Insets present EDS spectra (bottom) and Fourier transforms of high resolution images, with interplanar distances indicated in nm (top). Cu detected by EDS originates from the copper grid: (a) recomposed image of a typical aggregate of biopolymers with gel-like organic domains (arrows) and associated iron oxyhydroxides; (b) enlarged view of Figure 7a, showing ferrihydrite aggregate, according to its structure (HRTEM inset) and composition; (c) HRTEM of aggregate of ferrihydrite nanocrystallites with various orientations. Sample prepared from Cc fraction; (d) HRTEM of aggregate of oriented nanocrystalline iron oxides; and (e) colloidal euhedral kaolinites containing traces of iron.

Table 3. Input values used to model iron distribution in the different samples.

	Sample location	pH	Fe tot μmol/L	Al tot μmol/L	O.M. mg/L	Mg* μmol/L	Ca* μmol/L	Si μmol/L
Particulate fraction: P> 0.2 μ								
Rio Negro 10/98	RN Foz Rio Açai	4.1	1.0	1.6	1.3	2.5	3.75	60.7
Rio Negro 07/96	RN at Serrinha	4.4	11.8	11.8	8.0	1.56	3.66	124
Rio Negro 07/96	RN Foz Rio Branco	4	5.1	6.0	10.0	0.99	20.6	124
Rio Branco 10/97	Rio Branco	6.15	3.4	9.6	2.0	22.1	28.5	236
Rio Negro 10/98	RN at Moura	4.55	2.6	5.7	1.2	3.33	4.25	96.1
Rio Negro 10/96	RN at Moura	5	7.0	10.3	6.1	5.19	7.75	223
Rio Negro 07/96	RN at Moura	5.4	10.1	32.4	2.8	15.1	21	316
Rio Negro 10/97	RN at Moura	5.4	5.0	7.0	0.6	6.25	24.7	189
Rio Negro 10/97	RN at Moura	5.6	5.0	3.0	1.2	3.5	12.3	107
Rio Solimoes 10/97	Rio Solimões	6.38	9.3	22.9	1.0	58.3	253	224
Rio Trombetas 10/97	Rio Trombetas	5.89	29.3	109.0	2.0	13.3	27.3	144
Rio Amazon 10/97	Amazon at Obidos	6.78	10.0	27.9	2.0	67.1	189	259
Mengong 11/95	Mengong	5.3	203.0	—	452.0	24.7	32.5	254
Nyong 11/95	Nyong	5.9	18.0	—	8.0	21.8	30	175
Colloidal fraction: 0.2μ> Colloids>5000D								
Rio Negro 10/98	RN Foz Rio Açai	4.1	1.89	2.61	9.44	2.5	3.75	60.7
Rio Negro 07/96	RN at Serrinha	4.4	0.86	1.02	4.00	1.56	3.66	124
Rio Negro 07/96	RN Foz Rio Branco	4	0.86	1.02	3.43	0.99	20.6	124
Rio Branco 10/97	Rio Branco	6.15	0.28	0.29	4.67	22.1	28.5	236
Rio Negro 10/98	RN at Moura	4.55	1.66	2.04	6.88	3.33	4.25	96.1
Rio Negro 10/96	RN at Moura	5	0.28	0.30	1.80	5.19	7.75	223
Rio Negro 07/96	RN at Moura	5.4	0.57	0.66	3.00	15.1	21	316
Rio Negro 10/97	RN at Moura	5.4	0.76	0.66	5.71	6.25	24.7	189
Rio Negro 10/97	RN at Moura	5.6	0.61	0.66	6.29	3.5	12.3	107
Rio Solimoes 10/97	Rio Solimões	6.38	0.05	0.10	0.21	58.3	253	224
Rio Trombetas 10/97	Rio Trombetas	5.89	0.03	0.04	0.21	13.3	27.3	144
Rio Amazon 10/97	Amazon at Obidos	6.78	0.09	0.03	2.35	67.1	189	259
Mengong 11/95	Mengong	5.3	68	—	300	24.7	32.5	254
Nyong 11/95	Nyong	5.9	86	—	444	21.8	30	175

* Ca and Mg concentrations measured in the dissolved fraction. Values for Fe, Al, Si and the organic matter content (O.M.) are corrected by the concentration factor except for the Nyong and Mengong samples.

and low relative amount of this mineral confirm a negligible contribution of mineral, structural Fe in the analyzed colloids.

5.5. Geochemical Modeling of Fe Partition

The modeling of Fe speciation in the particulate and the colloidal fractions was made using the ECOSAT (Keiser and van Riemsdijk, 1999) code. This code includes the NICA-Donnan model that is used for the description of competitive metal ion binding to heterogeneous natural organic matter at different pH or ionic strength (Kinniburgh et al., 1999). Fe and Al concentrations in solution are assumed to be in geochemical equilibrium with hydrous ferric oxides (HFO, Ks = −38.6) and Kaolinite (Ks = −83.2), respectively. The modeling of the iron speciation in the colloidal fractions was made with the generic NICA-Donnan parameters for humic acids published by Milne et al. (2003). This choice is dictated by the results of our previous studies on the organic matter reactivity of the Rio Negro (Benedetti et al., 2002).

In addition to the samples studied here, we have used chemical data corresponding to the same rivers and the same locations, but sampled a different year or time of the same hydrological year. The input data used for the modeling are given in Table 3. Data for African river samples are taken from Viers et al. (2000) and Olivié-Lauquet et al. (1999, 2000). The data corresponding to the other Amazonian rivers samples are taken from Benedetti et al. (2003a) and Aucour et al. (2003).

The results of the calculations are given in Figure 9. The good agreement between calculated amounts of iron bound to organic matter and concentrations measured by EPR confirms previous hypothesis of Fox (1988) of an equilibrium control of the iron concentration in solution for riverine systems by colloidal HFO.

The same calculations were made for the particulate fractions using input data from Table 3. EPR information is only available for the Ps fractions. They have the same amount of iron associated with organic matter as the colloidal fractions (Cs) (Fig. 6). Thus, we assumed that all other data points for the particulate fraction should cluster on the same trend line as function of pH as observed for the colloidal fraction in Figure 6. With the binding constants used for the colloidal fraction, the calculated amounts of iron bound to particulate organic matter (not shown here) were generally two times higher than the amounts actually measured for the Ps fractions by EPR. To lower the amount of iron bound to the organic matter new calculations were made with smaller values for iron binding constants to carboxylic and phenolic type groups. When the constants are lowered by 2 orders of magnitude (i.e., −2 on a logK scale) the calculated points cluster nicely along the line corresponding to the colloidal fractions (Fig. 10). The lowering of the binding constants for the particulate fraction reflects a lower affinity for this fraction towards iron. A similar result was previously reported by Eyrolle et al. (1996) for copper in small tropical rivers. Changes in site density with size fractions

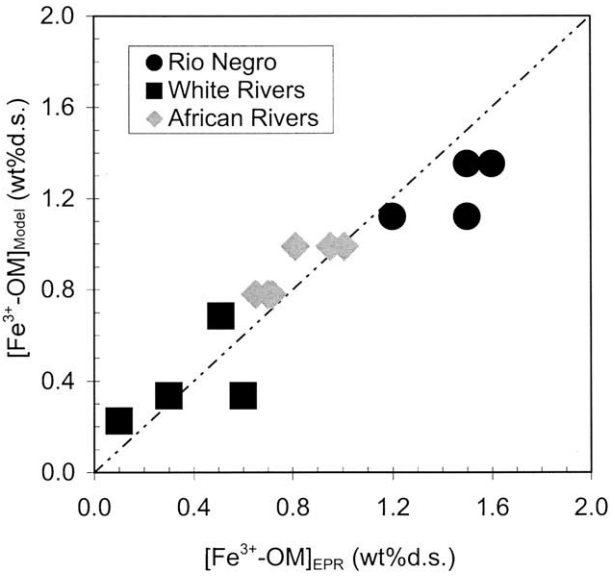

Fig. 9. Modeling of Fe sorption on colloidal organic matter as a function of pH, considering equilibrium with ferrihydrite (Ks = −38.6) and Fe binding to a generic humic acid.

could be related to the nature of the organic matter in each fraction. The colloidal fraction is likely to be composed of more "mature" organic material while the particulate fraction is made of less reactive, "younger" organic debris and decayed parts of organisms (Gadel et al., 2000). Differences could also result from in situ production of organic matter with chemical characteristics different from the soil derived organic matter (Degens et al., 1991). Further chemical characterization of the organic matter in the different samples is needed to test this hypothesis. However, the increase in site density for the colloidal fraction is consistent with findings on Cu(II) binding to soil humic substances. Town and Powell (1993) probed the Cu(II) binding capacity of soil derived humic and fulvic acids. These authors showed that soil humic acids have a higher affinity for copper than the fulvic acids. Moreover slightly different C/N ratios of the collected fractions could point to some dissimilarity in organic matter reactivity as shown recently by Croué et al. (2003).

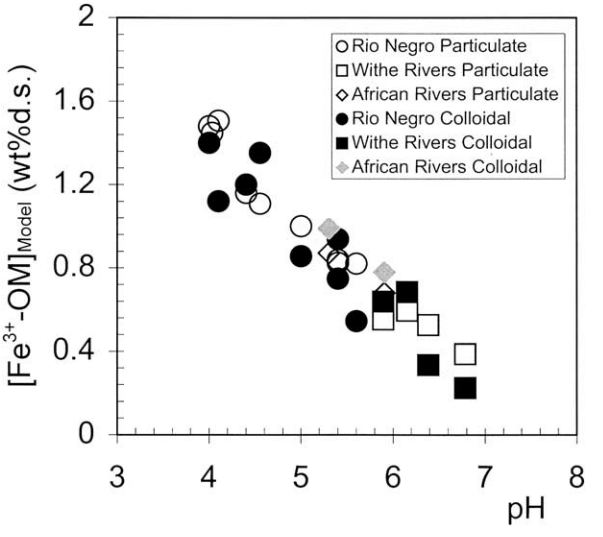

Fig.10. Modeling of Fe binding to particulate (Part.) and colloidal (Col.) organic matter as a function of pH considering equilibrium with ferrihydrite (Ks = −38.6) and Fe binding to a generic humic acid. Here the Fe binding affinity constants used in the NICA-Donnan model for carboxylic and phenolic type groups were lowered by -2 (logK) for particulate matter, to reach agreement between EPR results and calculations.

The bulk water speciation of iron in the different rivers can be derived from the model calculations and the respective amounts of particulate and colloidal iron. The result of the calculations given in Figure 11 indicates that iron in the mineral form (ferrihydrite) dominates in most rivers except the Rio Negro where, due to low pH and high organic matter concentration, the organic form is dominant. However, calculations also show strong seasonal variations on the iron speciation since the amount of iron bound to OM varies from 10 to 50% for samples taken at Moura in July 1996 (7/96) and in October 1998 (10/98), respectively.

6. DISCUSSION

6.1. Geochemical Significance of Colloidal Iron in Rivers from the Amazon Basin

In the Rio Negro, the similarities of species depicted by EPR between particulate organic (Ps) and colloidal fractions are related to similarities of iron complexes at molecular scale. The present data show that these colloidal materials can be differentiated through the content of iron bound to organic matter, a process controlled by the pH of the rivers. Considering results from Cameroon organic streams (Olivié-Lauquet et al., 2000), these iron paramagnetic species appear characteristic of natural organic matter such as humic substances in the studied systems. The type of functional group involved in trivalent iron binding is not differentiated through EPR. However, NICA-Donnan model calculations can be used to estimate the contribution of the two major reactive groups of natural organic matter (i.e., carboxylic and phenolic type groups). Calculations establish that as pH increases, the contribution of phenolic type groups to iron binding raises from 33 to 85% and concurrently the carboxylic type groups contribution decreases from 67 to 15%. Additionally, previous titration results showed that the reactivity of suspended material is consistent with carboxylic moieties in the pH range of the Rio Negro (4−4.5) (Allard et al., 2002; Benedetti et al., 2002). Except for dominant mineral components (e.g., kaolinite, quartz), the operationally defined fractions (particulate, colloidal, and related supernatants) are purely artificial with respect to the actual organic and mineral solid entities present in water samples. As a matter of fact, Field Flow Fractionation results of particulate and colloidal Rio Negro water samples suggested a continuum of aggregated small organic units of less than 1000 Daltons (Benedetti et al., 2002; Benedetti et al., 2003b). On the other hand, although the retention of some organic colloids in the particulate fraction by the filtration process cannot be excluded, the different Fe^{3+}-OM content, together with modeling results, suggest some dissimilarities in organic matter reactivity.

In addition to organic complexes, nanometric Fe oxides are also found in association to the particulate organic matter. This

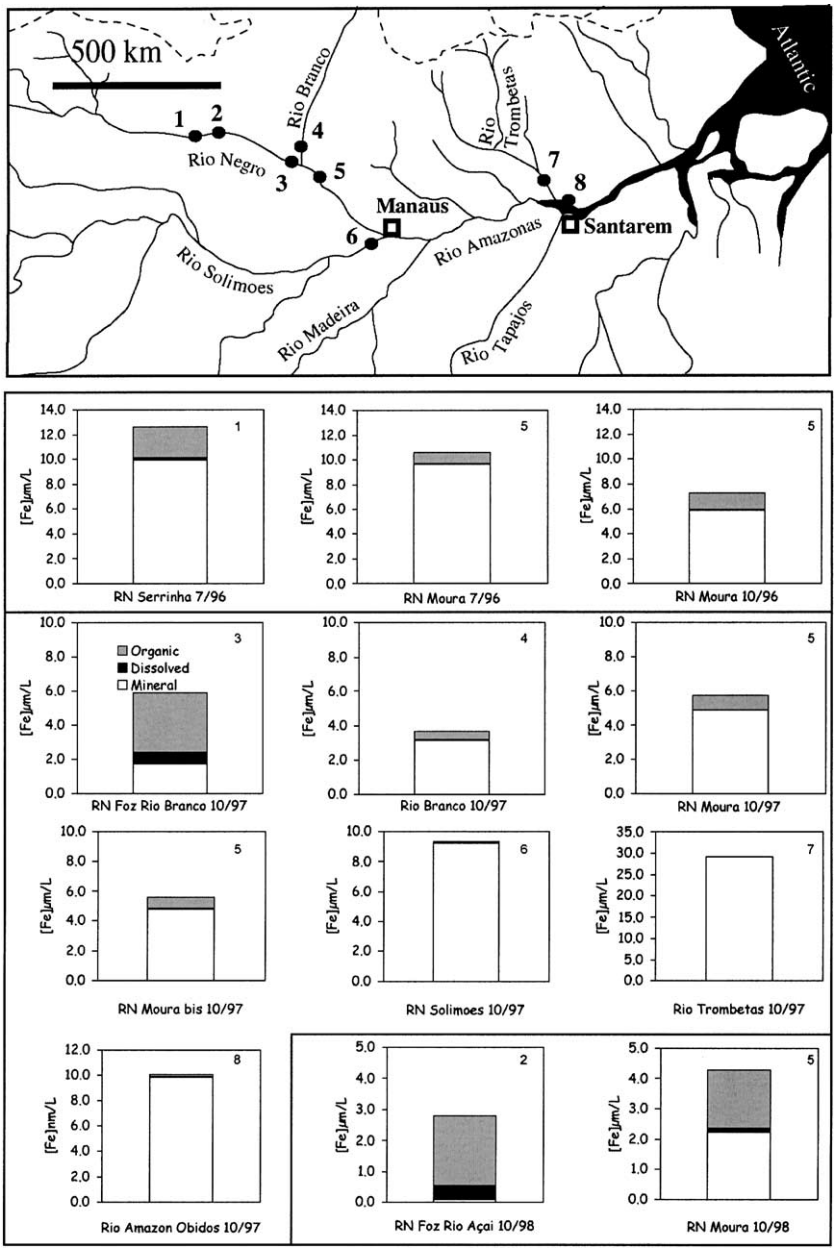

Fig. 11. Bulk iron speciation calculated for surface water samples taken at different times and locations in the major rivers of the Amazon Basin.

association is consistent with the relative surface charges of these compounds at the acidic pH of the Rio Negro. Indeed, below its zero point of charge (pHzpc ~ 7.9–8.1), the variable-surface charge of ferrihydrite is increasingly positive towards low pH (Buffle et al., 1998). On the other hand, the net surface charge of humic substances is negative in the range of natural pH (Swift, 1996).

The contrast in content of Fe associated with colloidal organic matter observed between the Rio Negro and the Amazon River is consistent with the major weathering processes occurring in the various drained pedoclimatic regions. In podzolic areas such as those drained by the Rio Negro, active processes favor relatively slow degradation of organic matter, organic binding of iron (and aluminum), and local precipitation of ferrihydrite in strongly depleted profiles (Dubroeucq and Volkoff, 1998). The related water chemistry is governed by acidity of organic matter and poor solute content (Lewis Jr et al., 1995). By contrast, dominantly ferrallitic areas such as those drained by other studied rivers are characterized by both strong degradation of organic matter and accumulation of iron within profiles (Fritsch et al., 2002). The sorption and filtering capacities of these clayey soils are high enough for percolating waters (clear waters) to carry negligible amounts of suspended material. In the case of the Rio Solimões and the Amazon River, both near neutral pH and presence of dissolved instead of colloidal organic matter (Mounier et al., 2002, Benedetti et

al., 2003a), are thus at the origin of the low [Fe^{3+}-OM] in colloidal material.

6.2. Implications for the Stability of Ferrihydrite in Rivers

The recognition of trivalent iron bound to organic matter and colloidal iron oxyhydroxides is in full agreement with the modeling by Tipping et al. (2002). Assuming a geochemical control of Fe content in solution by hydrous ferric oxides, the content of Fe bound to organic matter calculated from the ECOSAT code in the present study is consistent with the EPR measurements. In addition, TEM observations show the presence of ferrihydrite in the Rio Negro, although the presence of iron oxides and oxyhydroxides different from ferrihydrite cannot be excluded owing to the lack of experimental data, particularly in rivers other than the Rio Negro, owing to the lack of experimental data. The presence of ferrihydrite in rivers is an important issue considering the reactivity of these phases.

Ferrihydrite is a generic term for short ordered hydrous ferric oxides, with no single formula widely accepted (Cornell and Schwertmann, 1996). Its formation, commonly proceeding via oxidation of Fe(II) and subsequent Fe(III) hydrolysis, is kinetically favored when iron supply is high enough, through e.g., fast oxidation of Fe(II) at a redox front. The rate of redox iron cycling may be kinetically increased as a result of photochemical reactions locally providing Fe(II) supply (Waite and Morel, 1984; Voelker et al., 1997), or bacterial activity which may oxidize or reduce iron according to involved strains and environmental conditions (Warren and Haack, 2001). Thus, iron-rich biomineralizations associated with bacteria have been observed in the Rio Solimões but not in the Rio Negro (Konhauser et al., 1993). As mentioned by Davison and De Vitre (1992), although several possible pathways of Fe redox cycle have been determined, the dominant mechanisms actually effective in natural waters are still not identified. For instance, the formation of ferrihydrite is favored by the presence of Si (Schwertmann and Thalman, 1976). On the other hand, the presence of ferrihydrite in the Rio Negro samples can be maintained by poisoning of surfaces by impurities such as Si or organic molecules. As a matter of fact, it is known that both humic substances and silica may act as stabilizing agents for ferrihydrite in soil environments (Cornell and Schwertmann, 1996). Various experimental studies supported these observations by showing that organic compounds, silicate, and also sulfate anions retard or inhibit the conversion of ferrihydrite into more stable phases such as goethite or hematite (Jambor and Dutrizac, 1998). In addition, some TEM observations in this study suggest that organic structures may locally act as substrates for ferrihydrite growth. This is revealed only for organic fibrils for which spatial organization is solved, by contrast to gel-like organic domains for which no structural detail is obvious. Such a process of growth promoted by organic matter, previously proposed from TEM analysis of freshwater colloids (Perret et al., 2000), would increase the proportion of Fe occurring as nanosized oxides to the expense of complexed and soluble iron. Besides, the presence of mixed phases with different structures of individual crystallites evidenced from recent structural investigations (Janney et al., 2000a,b) would also influence ferrihydrite solubility, if such natural mixtures are found to vary in component proportions.

From the above discussion, one cannot specify the actual origin of ferrihydrite, i.e., either inherited from soils or freshly formed in the water column, as both forms remain possible. In addition, several factors may lower the effective reactivity and solubility of ferrihydrite. Nevertheless, as long as the above-mentioned factors affecting iron cycle in freshwater are not understood and properly modeled, it appears premature to verify the assumption of chemical equilibrium.

7. CONCLUSIONS

We have shown that by combining spectroscopic and microscopic observation techniques with available state-of-the-art modeling and bulk chemical analysis, it is possible to qualify and quantify the major forms of colloidal iron in rivers. EPR shows a decreasing trend of the content of Fe bound to organic matter as a function of increasing river pH. EPR and μPIXE data quantitatively confirm the presence of colloidal iron phase (min. 35 to 65% of iron content), assuming no divalent Fe is present. In the Rio Negro, HRTEM specifies the nature of colloidal iron phase as ferrihydrites particles of *circa* 20 to 50 Å associated with organic matter. The geochemical modeling results are in agreement with these experimental data and suggest an equilibrium solubility control between the mineral and the organic forms of iron. However, to extend the model to the particulate fraction, binding constants for the particulate fraction were lowered. This change could reflect a lower affinity of those fractions for iron. Extension of the model to the particulate fraction would finally allow one to calculate the speciation for the total amount of iron in the major rivers of the Amazon Basin.

Acknowledgments—This work was supported by the Programme Sol et Erosion (PROSE) from the Institut des Sciences de l'Univers of the CNRS, and the Institut de Recherche et de Developpement (IRD). The authors are grateful to E. Fritsch (IRD) for fruitful discussions on lateritic processes in the Amazon Basin. Cyril Girardin is thanked for C analyses of solids at the Laboratoire de Biogéochimie Isotopique (University Pierre & Marie Curie). The CP2M team is also acknowledged for the use of the Jeol 2010F TEM at the University of Aix-Marseille III. The authors express their gratitude to the Hidrologia de Bacia Amazonica project team (CNPq-IRD-ANEEL and UnB). D. Perret is acknowledged for his constructive review which improved the quality of the paper. Naziano, Marcos, Patrick et Jean-Loup merci, sans vous ceci n'aurait pas été possible. This is an IPGP contribution n° 1965. This is an INSU contribution n°358.

Associate editor: G. Sposito

REFERENCES

Allard T., Ponthieu M., Weber T., Filizola N., Guyot J. L., and Benedetti M. (2002) Nature and properties of suspended solids in the Amazon Basin. *Bull. Soc. Géol. France* **173,** 67–75.

Aucour A.-M., Tao F., Moreira-Turcq P., Seyler P., Sheppard S., and Benedetti M. F. (2003) The Amazon River. Behavior of metals (Fe, Al, Mn) and dissolved organic matter in the initial mixing at the Rio Negro/Solimões confluence. *Chem. Geol.* **197,** 271–285.

Balan E., Allard T., Boizot B., Morin G., and Muller J.-P. (1999) Structural Fe^{3+} in natural kaolinites: New insights from electron paramagnetic resonance spectra fitting at X and Q-band frequencies. *Clays Clay Miner.* **47,** 605–616.

Banfield J. F., Welch S. A., Zhang H., Ebert T. T., and Pen R. L. (2000) Aggregation-based crystal growth and microstructure development in natural iron oxyhydroxide biomineralization products. *Science* **289,** 751–754.

Benedetti M. F., Ranville J. F., Ponthieu M., and Pinheiro J. P. (2002) Field flow fractionation characterization and binding properties of particulate and colloidal organic matter from the Rio Amazon and Rio Negro. *Org. Geochem.* **33,** 269–279.

Benedetti M. F., Mounier S., Filizola N., Benaim J., and Seyler P. (2003a) Carbon and metal concentrations, size distributions and fluxes in major rivers of the Amazon Basin. *Hydrological Processes* **17,** 1363–1377.

Benedetti M. F., Ranville J. F., Allard T., Bednar A. J., and Menguy N. (2003b) The iron status in colloidal matter from the Rio Negro, Brasil. *Colloid Surf.* **A217,** 1–9.

Bigham J. M., Carlson L., and Murad E. (1994) Schwertmannite, a new iron oxyhydroxy-sulphate from Pyhäsalmi, Finland, and other localities. *Min. Mag.* **58,** 641–648.

Bigham J. M., Schwertmann U., Traina S. J., Winland R. L., and Wolf M. (1996) Schwertmannite and the chemical modeling of iron in acid sulfate waters. *Geochim. Cosmochim. Acta* **60,** 2111–2121.

Bonnin D., Muller S., and Calas G. (1982) Le fer dans les kaolins. Etude par spectrométries RPE, Mössbauer, EXAFS. *Bull. Minéral.* **105,** 467–475.

Buffle J. and van Leeuwen H. P. (1992) Environmental particles. In *Environmental Analytical and Physical Chemistry Series* Vol. 1, Lewis Publishers.

Buffle J., Wilkinson K. J., Stoll S., Filella M., and Zhang J. (1998) A generalized description of aquatic colloidal interactions: the three-colloidal component approach. *Environ. Sci. Technol.* **32,** 2887–2899.

Calas G. (1988) Electron paramagnetic resonance. In *Spectroscopic methods in mineralogy and geology* (ed. F. C. Hawthorne), Vol. 18, pp. 513–571, Mineralogical Society of America.

Clozel B., Allard T., and Muller J. P. (1994) Nature and stability of radiation-induced defects in natural kaolinites: new results and reappraisal of published works. *Clays Clay Miner.* **42,** 657–666.

Cornell R. M. and Schwertmann U. (1996) *The iron oxides. Structure, properties, reactions, occurrence and uses.* VCH.

Croué J-P., Benedetti M. F., Violleau D., and Leenheer J. A. (2003) Characterization and copper binding of humic and non humic organic matter isolated from the South Platte River: Evidence of the presence of nitrogeneous binding site. *Environ. Sci. Technol.* **37,** 328–336.

Davison W. and De Vitre R. (1992) Iron particles in freshwater. In *Environmental Particles* (ed. J. Buffle and H. P. van Leeuwen), Vol. 1, pp. 315–355, Lewis Publishers.

Degens E. T., Kempe S., Richey J. E. (1991) *Biogeochemistry of Major World Rivers.* Wiley & Sons.

Dubroeucq D. and Volkoff B. (1998) From Oxisols to Spodosols and Histosols: evolution of the soil mantles in the Rio Negro basin (Amazonia). *CATENA* **32,** 245–280.

Eyrolle F., Benedetti M., Benaim J., and Fevrier D. (1996) The distribution of colloidal and dissolved organic carbon, major elements and trace elements in small tropical catchments. *Geochim. Cosmochim. Acta* **60,** 3643–3656.

Fritsch E., Montes-Lauar C. R., Boulet R., Melfi A. J., Balan E., and Magat P. (2002) Lateritic and redoximorphic features in a faulted landscape near Manaus, Brazil. *Eur. J. Soil Sci.* **53,** 203–217.

Fortin D., Leppard G. G., and Tessier A. (1993) Characteristics of lacustrine diagenetic iron oxyhydroxides. *Geochim. Cosmochim. Acta* **57,** 4391–4404.

Fox L. E. (1988) The solubility of colloidal ferric hydroxyde and its relevance to iron concentrations in river water. *Geochim. Cosmochim. Acta* **52,** 771–777.

Gadel F., Serve L., Benedetti M., Da Cunha L. C. and Blazi J-L. (2000) Biochemical characteristics of organic matter in the particulate and colloidal fractions downstream of the rio Negro and Solimões rivers confluence. *Agronomie* **20,** 477–490.

Gibbs R. J. (1972) Water chemistry of the Amazon River. *Geochim. Cosmochim. Acta* **36,** 1061–1066.

Gibbs R. J. (1973) Mechanism of trace metal transport in rivers. *Science* **180,** 71–73.

Gibbs R. J. (1977) Transport phases of transition metals in the Amazon and Yukon rivers. *Geol. Soc. Am. Bull.* **88,** 829–843.

Goodman B. A. and Hall P. L. (1994) Electron paramagnetic spectroscopy. In *Clay Mineralogy:spectroscopic and chemical determinative methods* (ed. M. J. Wilson), pp. 173-225, Chapman & Hall.

Greffié C., Amouric M., and Parron C. (2001) HRTEM study of freeze-dried and untreated synthetic ferrihydrites: consequences of sample processing. *Clay Minerals* **36,** 381–387.

Hart B. T., Douglas G. B., Beckett R., Van Put A., and Van Grieken R. E. (1993) Characterization of colloidal and particulate matter transported by the Magela Creek system, Northern Australia. *Hydrological Processes* **7,** 105–118.

Hedges J. I., Hatcher P. G., Ertel J. E., and Meyers-Schulte K. J. (1992) A comparison of dissolved humic substances from seawater with Amazon river counterpart by ^{13}C NMR spectrometry. *Geochim. Cosmochim. Acta* **56,** 1753–1757.

Hedges J. I., Cowie G. L., Richey J. E., Quay P. D., Benner R., Strom M., and Forschey B. R. (1994) Origins and processing of organic matter in the Amazon river as indicated by carbohydrates and amino acids. *Limnol. Oceanogr.* **39,** 743–761.

IrionG. (1991) Minerals in rivers. In *Biogeochemistry of Major World Rivers* (ed. E. Degens et al.), pp. 265–281, John Wiley & Sons.

Jambor J. L. and Dutrizac J. E. (1998) Occurrence and constitution of natural and synthetic ferrihydrite, a widespread iron oxyhydroxide. *Chem. Rev.* **98,** 2549–2585.

Janney D. E., Cowley J. M., and Buseck P. R. (2000a) Structure of synthetic 2-line ferrihydrite by electron nanodiffraction. *Am. Miner.* **85,** 1180–1187.

Janney D. E., Cowley J. M., and Buseck P. R. (2000b) Transmission electron microscopy of synthetic 2- and 6-line ferrihydrite. *Clays Clay Miner.* **48,** 111–119.

Janney D. E., Cowley J. M., and Buseck P. R. (2001) Structure of synthetic 6-line ferrihydrite by electron nanodiffraction. *Am. Miner.* **86,** 327–335.

Keiser M. G. and van Riemsdijk W. H. (1999) ECOSAT: Equilibrium Calculation of Speciation and Transport, user manual. Version 4.7. Wageningen Agricultural University, The Netherlands..

Kinniburgh D. G., van Riemsdijk W. H., Koopal L. K., Borkovec M., Benedetti M. F., and Avena M. J. (1999) Ion binding to natural organic matter: competition, heterogeneity, stoichiometry and thermodynamic consistency. *Colloid Surf.* **A151,** 147–166.

Konhauser K. O., Fyfe W. S., Ferris F. G., and Beveridge T. J. (1993) Metal sorption and mineral precipitation by bacteria in two amazonian river systems: Rio Solimões and Rio Negro, Brazil. *Geol.* **21,** 1103–1106.

Leppard G. G. (1992) Evaluation of electron microscope techniques for the description of aquatic colloids. In *Environmental particles* (ed. J. Buffle and H. P. van Leeuwen), Vol. 1, pp. 231–289, Lewis Publishers.

Lewis Jr. W. M., Hamilton S. K. and Saunders III J. F. (1995) Rivers of Northern South America. In *River and Stream Ecosystems* (ed. C. E. Cushing et al.), Vol. 22, pp. 219–256, Elsevier.

Manceau A. and Charlet L. (1994) The Mechanism of Selenate Adsorption on Goethite and Hydrous Ferric Oxide. *J. Coll. Interf. Sci.* **168,** 87–93.

Martinelli L. A., Victoria R. L., Dematte J. L., Richey J. E., and Devol A. H. (1993) Chemical and mineralogical composition of Amazon river floodplain sediments, Brazil. *Appl. Geochem.* **8,** 391–402.

Mavrocordatos D. and Fortin D. (2002) Quantitative characterization of biotic iron oxides by analytical electron microscopy. *Am. Miner.* **87,** 940–946.

Maxwell J. A., Campbell J. D., and Teesdale W. J. (1989) The Guelph PIXE software package. *Nucl. Inst. and Meth.* **B43,** 218.

Mills M. S., Thurman E. M., Ertel J. and Thorn K. A. (1996) Organic geochemistry and sources of natural aquatic foams. In *Humic and Fulvic Acids* (ed. Gaffney et al.), Vol. 651, pp. 151–192, American Chemical Society.

Milne C. J., Kinniburgh D. G., van Riemsdijk W. H., and Tipping E. (2003) Generic NICA-Donnan Model Parameters for Metal-Ion Binding by Humic Substances. *Environ. Sci. Technol.* **37,** 958–971.

Molinier, M., Guyot, J-L., Callede, J., Guimaraes, V., Oliveira, E., Filizola, N. (1997) Hydrologie du bassin amazonien. In *Environnement et développement en Amazonie brésilienne* (ed. H. Thery), pp 24–41, Belin.

Mounier S., Benedetti M. F., Benaim J. Y. and Boulègue J. (2002) Organic matter size dynamics in the Amazon river. In *The Ecohydrology of South American Rivers and Wetlands* (ed. M.E. MacClain), IAHS Special publication N°6, pp. 25–34.

Muller J. P. and Calas G. (1993) Genetic significance of paramagnetic centers in kaolinites. In *Kaolin Genesis and Utilization* (eds. H. H. Murray et al.), pp. 261–289, The Clay Minerals Society.

Nelson D. W. and SommersL. E. (1996) Total Carbon, organic carbon and organic matter. In *Methods of Soil Analysis, Part 3-Chemical Methods* (ed. J. M. Bartels and J. M. Bigham), pp. 961–1069. SSSA Book Series n°5.

Olivié-Lauquet G., Allard T., Benedetti M., and Muller J. P. (1999) Chemical distribution of trivalent iron in riverine material from a tropical ecosystem: A quantitative EPR study. *Wat. Res.* **33,** 2726–2734.

Olivié-Lauquet G., Allard T., Bertaux J., and Muller J. P. (2000) Crystal chemistry of suspended matter in a tropical hydrosystem, Nyon Basin (Cameroon, Africa). *Chem. Geol.* **170,** 113–131.

Perret D., De Vitre R. R., Leppard G. G. and Buffle J. (1990) Characterizing autochthonous iron particles and colloids-the need for better particle analysis methods. In *Large Lakes. Ecological Structure and Function* (ed. M. M. Tilzer and C. Serruya), pp. 224–244. Springer-Verlag.

Perret D., Leppard G. G., Müller M., Belzile N., De Vitre R. R., and Buffle J. (1991) Electron microscopy of aquatic colloids: non-perturbing preparation of specimens in the field. *Wat. Res.* **25,** 1333–1343.

Perret D., Gaillard J. F., Dominik J., and Atteia O. (2000) The diversity of natural hydrous iron oxides. *Environ. Sci. Technol.* **34,** 3540–3546.

Schwertmann U. and Thalman H. (1976) The influence of [FeII] [Si], and pH on the formation of Lepidocrocite and Ferrihydrite during oxidation of aqueous $FeCl_2$ solutions. *Clay Minerals* **11,** 189–200.

Senesi N. (1992) Metal-humic substance complexes in the environment. Molecular and mechanistic aspects by multiple spectroscopic approach. In *Biogeochemistry of Trace Metals* (ed. D. C. Adriano), pp. 429-496. Lewis Publishers.

Sioli H. (1984) The Amazon. Limnology and landscape ecology of a mighty tropical river and its basin. In *Monographiae Biologicae*, (ed. H. J. Dumont), Vol. 56, pp. 763, DR W. Junk Publishers.

Swift R. S. (1996) Organic matter characterization. In *Methods of Soil Analysis, Part 3-Chemical Methods* (ed. J. M. Bartels and J. M. Bigham), pp. 1011-1069, SSSA Book Series n°5.

Tipping E., Rey-Castro C., Bryan S. E., and Hamilton-Taylor J. (2002) Al(III) and Fe(III) binding substances in freshwaters, and implications for trace metal speciation. *Geochim. Cosmochim. Acta* **66,** 3211–3224.

Town R. M. and Powell H. K. J. (1993) Ion-selective electrode potentiometric studies on the complexation of copper(II) by soil-derived humic and fulvic acids. *Anal. Chim. Acta* **279,** 221–233.

Viers J., Dupré B., Polvé M., Schott J., Dandurand J.-L., and Braun J.-J. (1997) Chemical weathering in the drainage basin of a tropical watershed (Nsimi-Zoetele site, Cameroon): comparison between organic-poor and organic-rich waters. *Chem. Geol.* **140,** 181–206.

Viers J., Dupré B., Braun J-J., Deberdt S., Angeletti B., Ndam Ngoupayou J., and Michard A. (2000) Major and trace element abundances, and strontium isotopes in the Nyong basin rivers Cameroon:constraints on chemical weathering processes and elements transport mechanisms in humid tropical environments. *Chem. Geol.* **1,** 69211–69241.

Voelker B. M., Morel F. M., and Sulzberger B. (1997) Iron Redox cycling in surface waters: effects of humic substances and light. *Environ. Sci. Technol.* **31,** 1004–1011.

Waite T. D. and Morel F. M. M. (1984) Photoreductive dissolution of colloidal iron oxides in natural waters. *Environ. Sci. Technol.* **18,** 860–868.

Warren L. A. and Haack E. A. (2001) Biogeochemical controls on metal behaviour in freshwater environments. *Earth-Sci. Rev.* **54,** 261–320.

Wells M. (1999) Manipulating iron availability in nearshore waters. *Limnol. Oceanogr.* **44,** 1002–1008.